Human Molecular Genetics, 2015, Vol. 24, No. 8 2163–2174

doi: 10.1093/hmg/ddu736
Advance Access Publication Date: 30 December 2014
Original Article

ORIGINAL ARTICLE

Neurofilament light polypeptide gene N98S mutation in mice leads to neurofilament network abnormalities and a Charcot-Marie-Tooth Type 2E phenotype

Adijat A. Adebola[1,2,†], Theo Di Castri[1,†], Chui-Zhen He[1,†], Laura A. Salvatierra[1,†], Jian Zhao[1,†], Kristy Brown[1], Chyuan-Sheng Lin[1,2], Howard J. Worman[1,3] and Ronald K.H. Liem[1,2,*]

[1]Department of Pathology and Cell Biology, [2]Taub Institute for Research in Alzheimer's Disease and the Aging Brain and [3]Department of Medicine, Columbia University Medical Center, 630 West 168th Street, New York, NY 10032, USA

*To whom correspondence should be addressed. Tel: +1 2123054078; Fax: +1 2123055498; Email: rkl2@cumc.columbia.edu

Abstract

Charcot-Marie-Tooth disease (CMT) is the most commonly inherited neurological disorder with a prevalence of 1 in 2500 people worldwide. Patients suffer from degeneration of the peripheral nerves that control sensory information of the foot/leg and hand/arm. Multiple mutations in the neurofilament light polypeptide gene, *NEFL*, cause CMT2E. Previous studies in transfected cells showed that expression of disease-associated neurofilament light chain variants results in abnormal intermediate filament networks associated with defects in axonal transport. We have now generated knock-in mice with two different point mutations in *Nefl*: P8R that has been reported in multiple families with variable age of onset and N98S that has been described as an early-onset, sporadic mutation in multiple individuals. $Nefl^{P8R/+}$ and $Nefl^{P8R/P8R}$ mice were indistinguishable from $Nefl^{+/+}$ in terms of behavioral phenotype. In contrast, $Nefl^{N98S/+}$ mice had a noticeable tremor, and most animals showed a hindlimb clasping phenotype. Immunohistochemical analysis revealed multiple inclusions in the cell bodies and proximal axons of spinal cord neurons, disorganized processes in the cerebellum and abnormal processes in the cerebral cortex and pons. Abnormal processes were observed as early as post-natal day 7. Electron microscopic analysis of sciatic nerves showed a reduction in the number of neurofilaments, an increase in the number of microtubules and a decrease in the axonal diameters. The $Nefl^{N98S/+}$ mice provide an excellent model to study the pathogenesis of CMT2E and should prove useful for testing potential therapies.

Introduction

Charcot-Marie-Tooth disease (CMT) or hereditary motor and sensory neuropathies are inherited peripheral neuropathies caused by mutations in multiple genes (1–3). CMT is a prevalent disorder, with ~1 in 2500 people affected in the general population. CMT is caused by mutations in as many as 50 different genes and is generally divided into type 1 (CMT1) and type 2 (CMT2). CMT1 is primarily a demyelinating neuropathy caused by mutations in peripheral myelin proteins. CMT2 is caused by mutations in genes that affect the peripheral axon. The phenotypes are similar, but nerve conduction velocities are reduced in CMT1. In CMT2, the conduction velocities are fairly normal, although compound muscle action potentials are reduced (4,5).

Causative mutations have been identified in ~40% of CMT2 patients (6), although the first CMT2 gene was not identified until 2001. This is the neurofilament light polypeptide gene

† These authors contributed equally to this work.

Received: September 22, 2014. **Revised:** November 28, 2014. **Accepted:** December 22, 2014

© The Author 2014. Published by Oxford University Press. All rights reserved. For Permissions, please email: journals.permissions@oup.com

(*NEFL*) that encodes neurofilament light polypeptide (NFL), one of the neuronal intermediate filaments (IFs) forming the major cytoskeletal structure of the axon. Neuronal IFs consist of the neurofilament triplet proteins (called NFL, NFM and NFH for neurofilament light, middle and high), α-internexin and peripherin (7). The first *NEFL* mutations shown to cause CMT2E were dominantly inherited and led to amino acid substitutions in the head domain (P8R) and the rod domain (Q333P, now called Q334P) of NFL (8,9). Since then, a total of 14 mutations in *NEFL* have been reported in familial and sporadic cases of CMT. Although these mutations are generally considered to cause CMT2E, there are a number of cases of patients with *NEFL* mutations that resemble CMT1 (8). In these cases, there was a pronounced slowing in nerve conduction velocity, not generally observed in CMT2. In addition, there are two reports of recessive mutations that cause truncation of the NFL protein, resulting in loss of function leading to a severe form of CMT (10,11).

Neurofilaments, like all IFs, are composed of three major domains: an α-helical rod domain flanked by N-terminal head and C-terminal tail domains (7). The α-helical rod domain is necessary for the formation of a coiled-coil dimer, which is the first step in IF assembly. The head domain is generally considered more important for filament formation than the tail domain (12). The N98S mutation is in the rod domain, and transfection studies have shown that abnormal structures are formed both in the absence and in the presence of NFM (13). The P8R mutation is in the head domain and also does not self-assemble into a filamentous network. However, the mutant P8RNFL protein forms abnormal bundled filamentous structures in the presence of NFM in transfected cells (14). Both N98S and P8RNFL also disrupt the normal formation of filaments in cultured cells expressing wild-type (WT) NFL, consistent with the dominant inheritance observed in patients. Neurons from human subjects with other *NEFL* mutations have been reported to show giant axons, axonal swellings and myelinated fibers consisting exclusively of microtubules with few or absent neuronal IFs (15). In general, there appears to be a correlation between the effects of CMT2E-associated NFL variants on neuronal IF misassembly when expressed in transfected cells and the reported pathogenicity of the corresponding *NEFL* mutations in patients (13). The P8R mutation has been described in a number of families with variable ages of onset and severity of symptoms. The N98S mutation is sporadic with an early age of onset (8,10,16). The first reported N98S patient had an age of onset of <1 year and global developmental delay (8). In a subsequent study, two cases were reported, one with an age of onset of <1 year and another with an age of onset of <2 years. In addition to delayed walking and gait problems, these two patients both had hearing problems and one also had mental retardation (10).

These previous findings suggest that altered neuronal IF networks contribute to the pathogenic mechanisms leading to CMT2. However, no studies have been or can be done to correlate anatomy or histology with disease onset in humans, and there are no published autopsy reports of CMT2E patients. To circumvent this limitation, we have generated knock-in mouse models for CMT2E with the P8R and N98S *Nefl* mutations.

Results

Generation of *Nefl* P8R and N98S knock-in mice

We chose to generate mutations in the orthologous mouse *Nefl* gene using a knock-in strategy (Fig. 1A). This approach is 'physiological' in that the mutant allele is expressed at normal endogenous levels. We obtained multiple founders for the $Nefl^{P8R/+}$ and $Nefl^{N98S/+}$ mouse lines (Fig. 1B). Mice of both lines were fertile and have been backcrossed with C57BL/6 $Nefl^{+/+}$ mice for six generations. The $Nefl^{P8R/+}$ mice have also been bred to homozygocity ($Nefl^{P8R/P8R}$). Brains and spinal cords of the mice were analyzed to determine whether there were any large changes in mRNA and protein levels of the NFL variants. No significant changes in mRNA levels were observed in the $Nefl^{N98S/+}$ mouse lines by RT–PCR experiments (Fig. 1C). NFL protein levels were lower in the brain and spinal cord of all the mutant mice, with the greatest decrease (50–60%) in $Nefl^{P8R/P8R}$ mice compared with $Nefl^{+/+}$ mice (Fig. 1D and E). There was also an ~30% decrease in total NFL protein in the brains and spinal cord of the $Nefl^{N98S/+}$ mice. The level of total NFL protein levels in the sciatic nerves of the $Nefl^{N98S/+}$ mice exhibited a decrease of ~80% compared with the WT mice. Since no specific antibodies to the mutant proteins are available, these results only showed differences in total (mutant and WT) NFL protein.

$Nefl^{n98s/+}$ mice have abnormal hindlimb posture and tremor

$Nefl^{N98S/+}$, $Nefl^{P8R/+}$ and $Nefl^{P8R/P8R}$ mice all had normal growth rates and lifespans and were able to reproduce. The $Nefl^{N98S/+}$ mice showed a noticeable tremor and abnormal hindlimb posture that varied from a hitching motion when lifted by the tail to clasping (Fig. 2A and B). There were no differences between male and female animals. More than 85% of the $Nefl^{N98S/+}$ animals showed tremor and >50% of the $Nefl^{N98S/+}$ animals showed the clasping phenotype (Fig. 2C and D). To determine the age of onset that the animals start to shake and clasp, we pooled the mice at ages 1–3 months, 4–9 months and >9 months and found that the symptoms were already apparent at the earliest age tested and persisted throughout (Fig. 2C and D). To determine whether lack of complete penetrance of the phenotypes was due to the genetic background, we backcrossed the mice with C57Bl/6 WT mice more than six generations and tested these animals. For mutant mice of the C57BL/6 background, 97% were shaking, which was more than the 82% of the mice on a mixed background (Fig. 2E). There was no clear difference in the percentage of animals that were clasping (mixed: 56%; backcrossed: 49%) after backcrossing (Fig. 2F). In contrast to the marked phenotypes in the $Nefl^{N98S/+}$ mice, the $Nefl^{P8R/+}$ and $Nefl^{P8R/P8R}$ mice were indistinguishable from $Nefl^{+/+}$ mice with regards to both shaking and clasping up to 2 years of age.

Mutant N98S NFL protein forms aggregates in the spinal cord

Labeling of sections from spinal cord of 18-month-old mice with anti-NFL antibody showed abnormalities both in the anterior and in the posterior regions of the spinal cord (Fig. 3). In both regions of the $Nefl^{N98S/+}$ mice, we observed neurofilamentous aggregates in the neuronal cell bodies in the gray matter (GM) (Fig. 3B and D), which were not stained with anti-NFL in $Nefl^{+/+}$ mice (Fig. 3A and C). Axonal processes were stained in the white matter (WM) of the $Nefl^{+/+}$ mice (Fig. 3A and C), but there was comparatively little axonal labeling in the $Nefl^{N98S/+}$ mice, except that large neurofilament positive aggregates could be observed (arrows). In contrast, no aggregates were observed in either the $Nefl^{P8R/+}$ or $Nefl^{P8R/P8R}$ mice at 18 months of age (Supplementary Material, Fig. S1), although the intensity of labeling appeared to be lower in sections from these mice compared with sections from the $Nefl^{+/+}$ mice, consistent with the somewhat lower levels of total NFL protein (Fig. 1). The aggregates in the spinal cords of the

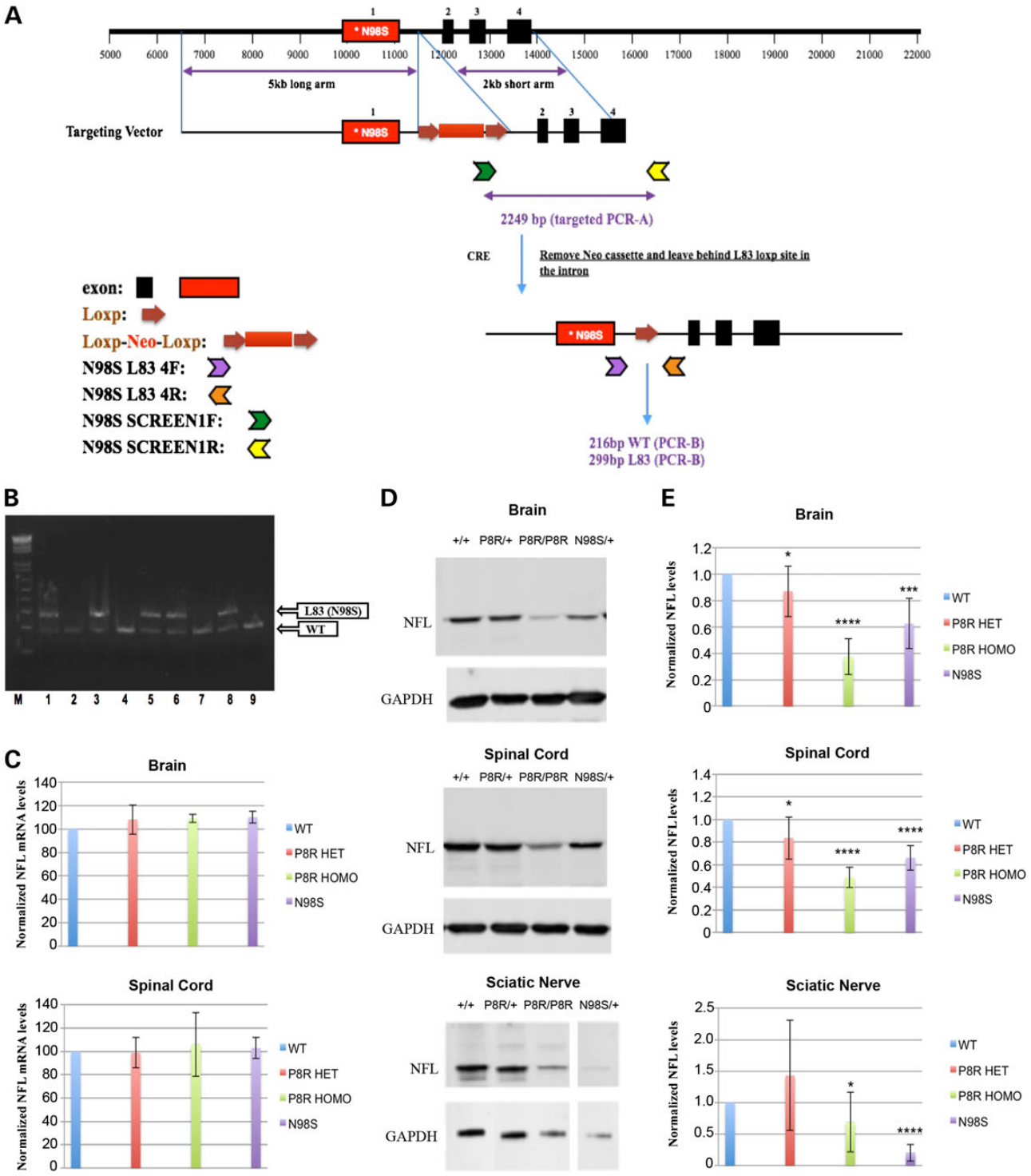

Figure 1. Generation of *Nefl* P8R and N98S knock-in mice. (**A**) Strategy for generating the knock-in mice: a targeting vector containing the point mutation in the first exon of *Nefl*, and a Loxp-Neo-Loxp cassette inserted in the first intron was constructed and used to generate the knock-in mice. The targeted allele could be differentiated from the WT allele by PCR using the 4F and 4R primers. (**B**) Ethidium bromide-stained agarose gel of PCR analyses of the F1 mice showing the WT and targeted (L83 (N98S)) alleles; five of the nine animals showed both alleles, the other four were WT. (**C**) RNA was isolated from brains and spinal cords of $Nefl^{+/+}$, $Nefl^{P8R/+}$ $Nefl^{P8R/P8R}$ and $Nefl^{N98S/+}$ mice and the amount of NFL mRNA was quantified by RT–PCR and compared with glyceraldehyde 3-phosphate dehydrogenase (GAPDH) mRNA. Ratios of NFL mRNA and GAPDH mRNA for the different genotypes are shown. Experiments were repeated with three sets of animals. (**D**) Western blots of brain, spinal cord and sciatic nerve from $Nefl^{+/+}$, $Nefl^{P8R/+}$, $Nefl^{P8R/P8R}$ and $Nefl^{N98S/+}$ probed with anti-NFL-N antibody and anti-GAPDH. (**E**) Ratios of NFL/GAPDH from the western blots shown in D. (Brain: $Nefl^{+/+}$: $n = 10$; $Nefl^{P8R/+}$: $n = 9$; $Nefl^{P8R/P8R}$: $n = 10$; $Nefl^{N98S/+}$: $n = 9$; Spinal cord: $Nefl^{+/+}$: $n = 10$; $Nefl^{P8R/+}$: $n = 9$; $Nefl^{P8R/P8R}$: $n = 10$; $Nefl^{N98S/+}$: $n = 9$; Sciatic nerve: $Nefl^{+/+}$: $n = 9$; $Nefl^{P8R/+}$: $n = 8$; $Nefl^{P8R/P8R}$: $n = 9$; $Nefl^{N98S/+}$: $n = 7$). Significance was calculated using a one-tailed, type 3 t-test in excel ($^{*}P \leq 0.05$, $^{***}P \leq 0.001$, $^{****}P \leq 0.0001$).

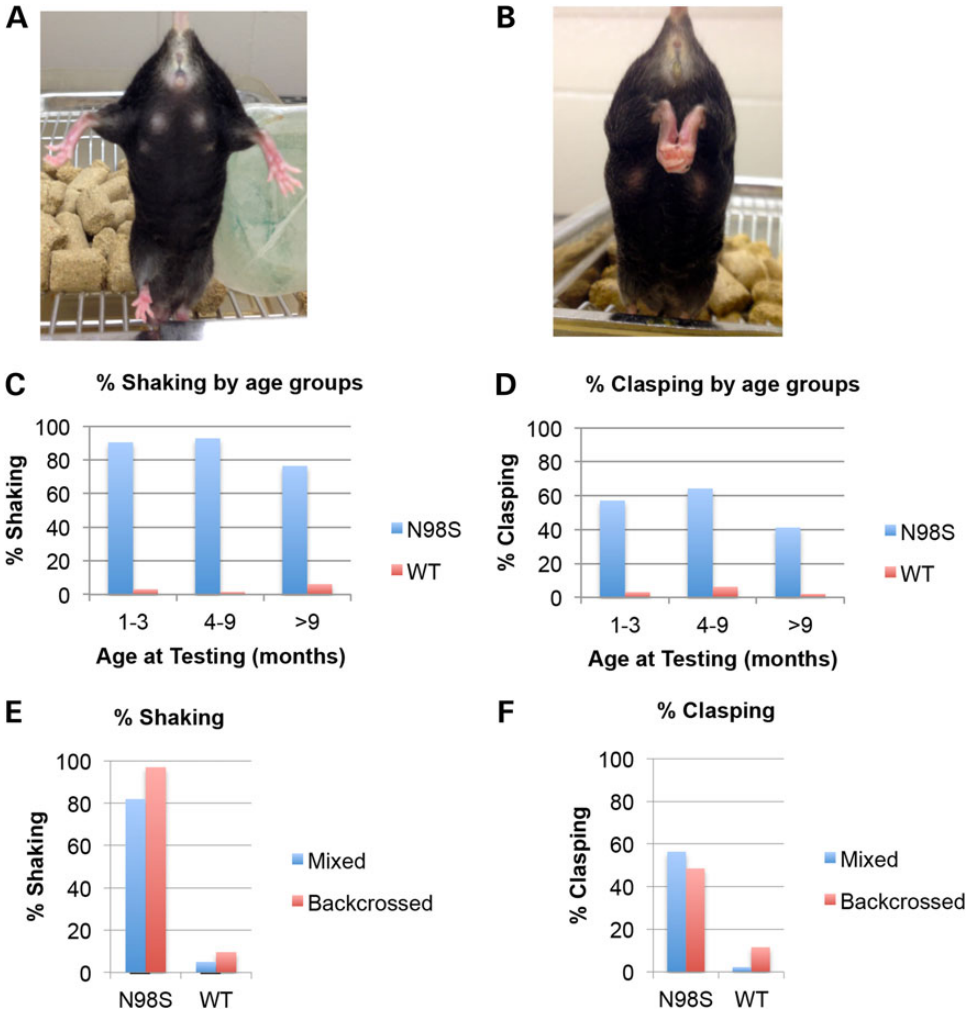

Figure 2. Abnormal hindlimb posturing and tremor in *Nefl*$^{N98S/+}$ mice. (**A**) Photograph of *Nefl*$^{+/+}$ mouse showing normal hindlimb posturing when suspended by its tail. (**B**) Photograph of *Nefl*$^{N98S/+}$ mouse showing abnormal hindlimb posturing (clasping) when suspended by its tail. (**C**) Percentages of *Nefl*$^{N98S/+}$ mice (blue bars) and *Nefl*$^{+/+}$ (WT) mice (red bars) that were shaking in different age groups. (**D**) Percentages of *Nefl*$^{N98S/+}$ mice (blue bars) and *Nefl*$^{+/+}$ (WT) mice (red bars) demonstrating hindlimb clasping in different age groups. (**E**) Blue bars: percentage of mice that were shaking before backcrossing to C57Bl6 mice five times; red bars: percentage of mice that were shaking after backcrossing five times. The proportion of *Nefl*$^{N98S/+}$ mice that exhibited shaking increased after backcrossing. (**F**) Red bars: percentage of mice showing hindlimb clasping before backcrossing to C57Bl6 mice five times; red bars: percentage of mice that show hindlimb clasping after backcrossing. (*Nefl*$^{N98S/+}$: before backcrossing $n = 71$, after backcrossing $n = 33$; *Nefl*$^{+/+}$: before backcrossing $n = 179$; after backcrossing, $n = 52$).

Nefl$^{+/+}$ mice were also positive for NFM (Supplementary Material, Fig. S2A and B).

Neurofilamentous aggregates in the dorsal root ganglia

Immunolabeling of dorsal root ganglia from 1-year-old mice with anti-NFL antibody shows cell body and process labeling in sections from WT mice (Fig. 4A and C). At high power, the cell body labeling appears to be filamentous (Fig. 4C). In contrast, the axonal labeling of the *Nefl*$^{N98S/+}$ mice was discontinuous and showed the presence of aggregates (Fig. 4B). In the cell bodies, the labeling pattern also showed discontinuous aggregates (Fig. 4D). The labeling pattern of NFM was the same as that of NFL (Supplementary Material, Fig. S2C and D). Labeling of the axons with NFM was also coincident with the NFL labeling (not shown).

Cerebellar abnormalities in *Nefl*$^{N98S/+}$ mice

We observed abnormal labeling with inclusions and abnormal processes in the cerebellum of an 18-month-old *Nefl*$^{N98S/+}$ mouse (Fig. 5). In WT animals, we observe Purkinje cell processes in the granular layer and basket cells processes around the Purkinje cell bodies that are all stained with anti-NFL (Fig. 5A). In contrast, we observed abnormal NFL-positive processes throughout the granular layer, with little labeling of the axons in the WM tract in the cerebella or the basket cell processes of the *Nefl*$^{N98S/+}$ mice (Fig 5B). The abnormal processes in the granular layer were reminiscent of cerebellar torpedoes that we previously observed in transgenic mice that overexpressed α-internexin (17). Cerebellar torpedoes are observed in the axons of the Purkinje cells and their presence correlates with essential tremor in humans (18). In α-internexin transgenic mice, abnormal filamentous inclusions in torpedoes correlated with malfunctioning and degeneration of Purkinje cells (17). To determine whether the abnormal processes in the cerebellum of *Nefl*$^{N98S/+}$ mice were torpedoes in the Purkinje cell axons, we performed double labeling with anti-calbindin, which labels Purkinje cells and their processes (19). Double labeling with anti-NFL and anti-calbindin antibodies suggested that the abnormal processes were not cerebellar torpedoes, but rather other disorganized processes in the cerebellum

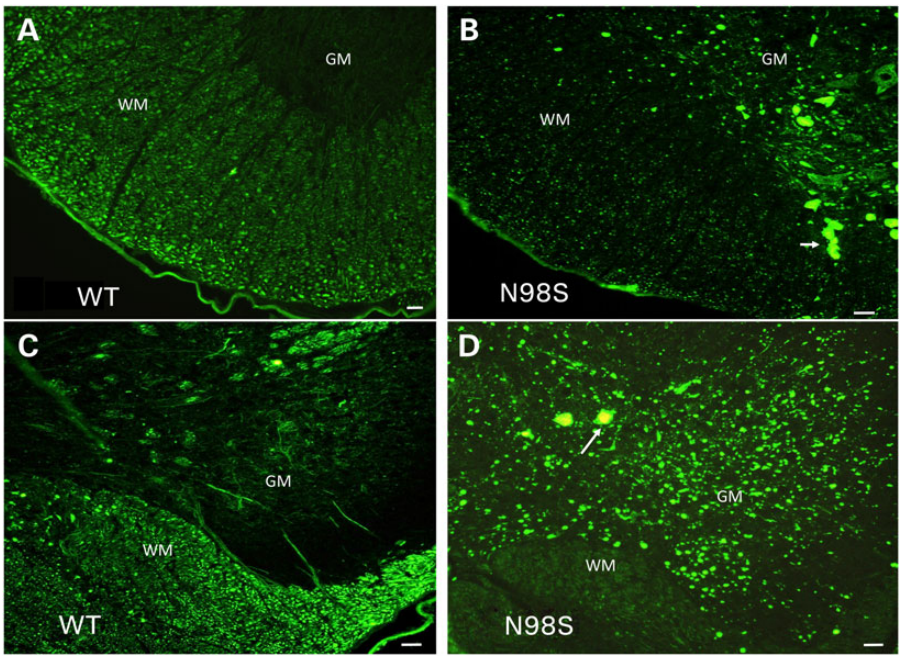

Figure 3. Immunofluorescence micrographs of sections of spinal cord stained with anti-NFL-N antibody showing inclusions in *Nefl*$^{N98S/+}$ mice. (**A**) Section of anterior horn of 18-month-old *Nefl*$^{+/+}$ (WT) mouse. (**B**) Section of anterior horn of 18-month-old *Nefl*$^{N98S/+}$ (N98S) mouse. (**C**) Section of posterior horn of 18-month-old *Nefl*$^{+/+}$ (WT) mouse. (**D**) Section of posterior horn of 18-month-old mutant *Nefl*$^{N98S/+}$ (N98S) mouse. WM of *Nefl*$^{+/+}$ mice shows axonal labeling, whereas there is relatively little labeling in the cell bodies of the GM in both the anterior and posterior horns. In contrast, there was relatively little labeling in the WM of *Nefl*$^{N98S/+}$ mice, except for the inclusions (arrow), which are likely due to axonal swellings. Inclusions are also observed in the GM in both the anterior and posterior sections (arrows). Bars = 50 μm.

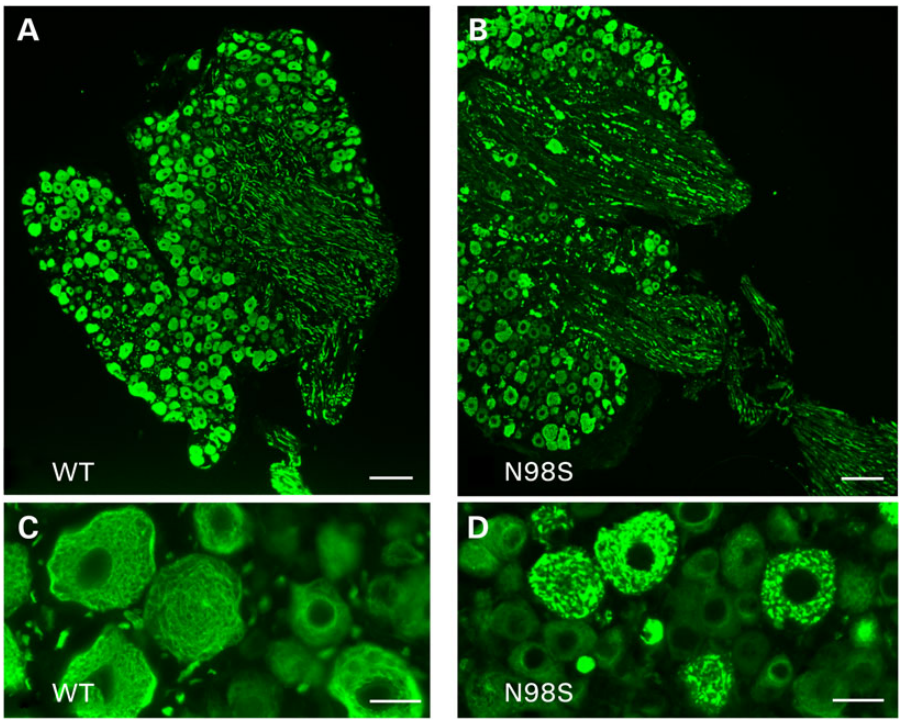

Figure 4. Immunofluorescence of sections of dorsal root ganglia showing abnormalities in *Nefl*$^{N98S/+}$ mice. (**A** and **C**) Labeling of dorsal root ganglia of WT mice; (**B** and **D**) Labeling of dorsal root ganglia of *Nefl*$^{N98S/+}$ mice. The cell bodies of the DRGs are stained with anti-NFL, and aggregates in the cell bodies can clearly be seen in the sections from the *Nefl*$^{N98S/+}$ mice. The processes from the *Nefl*$^{N98S/+}$ mice show a discontinuous staining with apparent aggregates. Bars (A and B) = 100 μm; (C and D) = 25 μm.

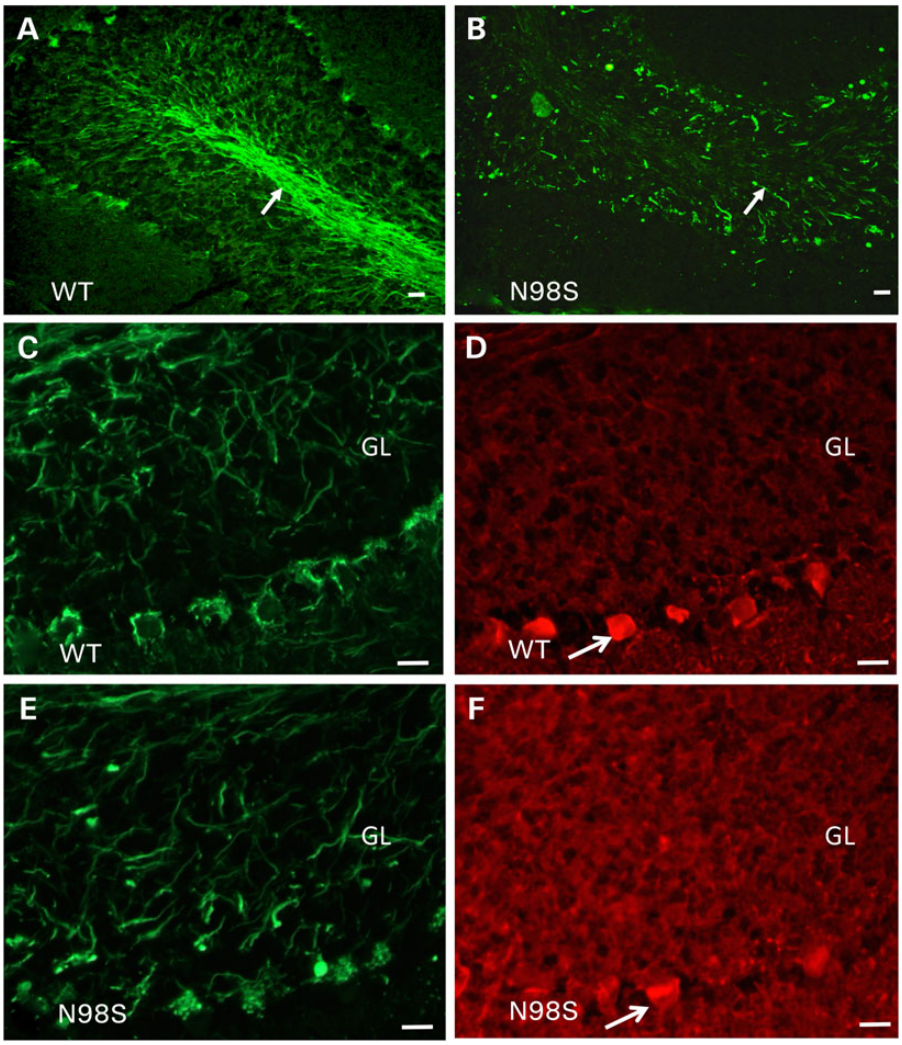

Figure 5. Immunofluorescence micrographs of sections of cerebellum showing abnormalities in *Nefl*$^{N98S/+}$ mice. (**A**) Labeling of the cerebellum of 18-month-old *Nefl*$^{+/+}$ (WT) mouse with anti-NFL-N antibody. (**B**) Labeling of the cerebellum of 18-month-old *Nefl*$^{N98S/+}$ (N98S) mouse with anti-NFL-N antibody. Note labeling of the WM tract in the *Nefl*$^{+/+}$ mouse compared with the irregular labeling and the absence of the WM tract in the cerebellum of the *Nefl*$^{N98S/+}$ mouse (arrows in A and B). There are also abnormal processes in the granular layer (GL) in the cerebellum of the *Nefl*$^{N98S/+}$ mouse. (**C** and **D**) Double labeling of cerebellar section from 18-month old *Nefl*$^{+/+}$ mouse with anti-NFL-N (green) and anti-calbindin (red) antibodies. (**E** and **F**) Double labeling of cerebellar section from 18-month-old *Nefl*$^{+/+}$ mouse with anti-NFL-N (green) and anti-calbindin (red) antibodies. Arrows indicate labeling of basket cell axons around the Purkinje cells in WT mice (C). In *Nefl*$^{N98S/+}$ mice, note the absence of basket cell process labeling (arrow) and the swellings in the GL of the cerebellum (E). The absence of calbindin labeling (F) suggests that they are not Purkinje cell processes but rather disordered basket cell processes. Bars = 50 μm.

(Fig. 5C–F). In the *Nefl*$^{P8R/+}$ mice, we did not observe any abnormal processes in the cerebellum. We also stained the pons and cerebral cortex of the *Nefl*$^{+/+}$ and *Nefl*$^{N98S/+}$ mice. In the pons, the strong axonal labeling observed in sections from a *Nefl*$^{+/+}$ mouse was not observed in sections from a *Nefl*$^{N98S/+}$ mouse. Instead there appeared to be punctate labeling throughout these processes (Supplementary Material, Fig. S3). There also appeared to be more punctate labeling in the cerebral cortex *Nefl*$^{N98S/+}$ compared with *Nefl*$^{+/+}$ mice, although there were no obvious inclusions (Supplementary Material, Fig. S4).

Developmental study of the *Nefl*$^{N98S/+}$ mice

The first immunohistochemical analyses were performed on sections from 18-month-old mice. However, because symptoms can be seen as early as 1 month, we performed labeling on the spinal cords and cerebella of mice at several different ages. Differences in the spinal cord were observed as early as 7 days, and they appeared to progressively worsen with age. In both the anterior and posterior spinal cords of 7-day-old mice, there was less labeling in the WM of the mutant animals compared with *Nefl*$^{+/+}$ (Fig. 6). In the GM, we observed NFL labeling in cell bodies in the *Nefl*$^{N98S/+}$animals, which was not observed in the *Nefl*$^{+/+}$ mice (Fig. 6A and B). These results suggest that neurofilaments started to accumulate in the cell bodies at this age, although they were not forming aggregates. There was some labeling in the WM of the posterior section, although the labeling was not as extensive as in sections from a *Nefl*$^{+/+}$ mouse (Fig. 6C and D). In sections from a 4-month-old *Nefl*$^{N98S/+}$ mouse, we observed less labeling in the WM and more dotted labeling in the GM. We also discerned some cell bodies with strong neurofilament labeling (Supplementary Material, Fig. S5). We did not observe as many inclusions

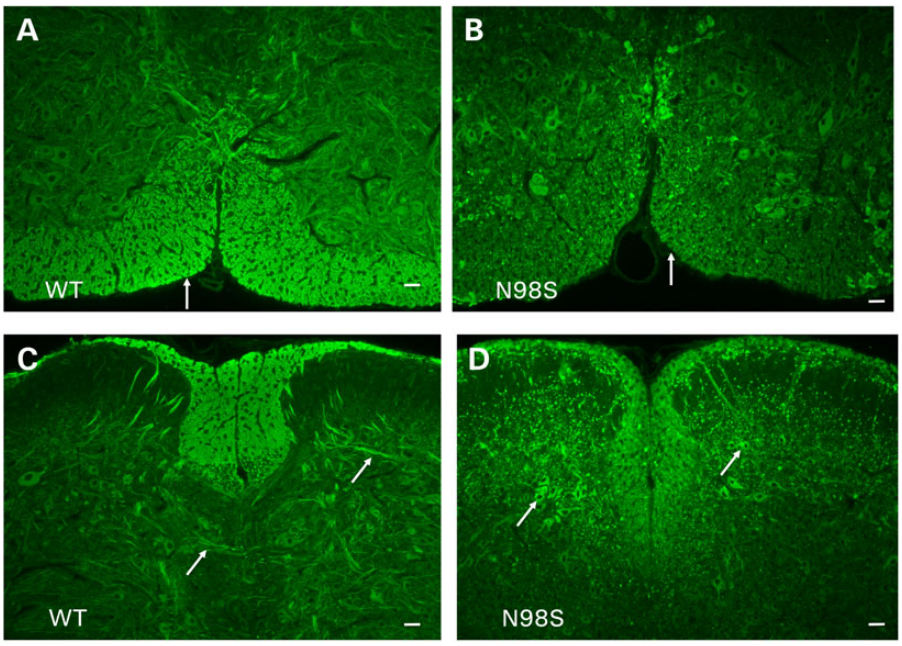

Figure 6. Immunofluorescence micrographs showing labeling of a post-natal day 7 spinal cords of *Nefl*$^{+/+}$ (WT) and *Nefl*$^{N98S/+}$ (N98S) with anti-NFL-N antibody. (**A**) Section of anterior horn from *Nefl*$^{+/+}$ mouse. (**B**) Section of anterior horn from *Nefl*$^{N98S/+}$ mouse. (**C**) Section of posterior horn from *Nefl*$^{+/+}$ mouse. (**D**) Section of posterior horn from *Nefl*$^{N98S/+}$ mouse. Arrows in A and B indicate the abundant axonal labeling of the WM of the *Nefl*$^{+/+}$ sections, which is reduced in the *Nefl*$^{N98S/+}$ sections. In the GM, axonal tracts can be observed in *Nefl*$^{+/+}$ sections (arrows, C), whereas prominent cell body labeling is observed in the posterior horn section from the *Nefl*$^{N98S/+}$ mouse (arrows, D). Bars = 50 μm.

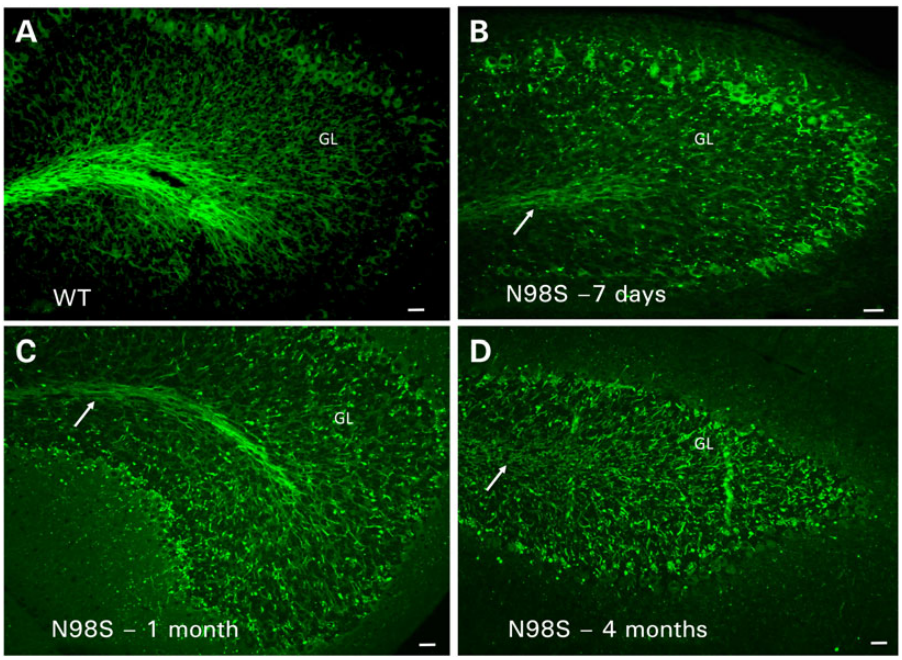

Figure 7. Immunofluorescence micrographs showing labeling with anti-NFL-N antibody of sections of cerebella from *Nefl*$^{+/+}$ and *Nefl*$^{N98S/+}$ mice of various ages. (**A**) Section of cerebellum from a 7-day-old *Nefl*$^{+/+}$ (WT) mouse. (**B**) Section of cerebellum from a 7-day-old *Nefl*$^{N98S/+}$ (N98S) mouse. (**C**) Section of cerebellum from a 1-month-old *Nefl*$^{N98S/+}$ (N98S) mouse. (**D**) Section of cerebellum from a 4-month-old *Nefl*$^{N98S/+}$ (N98S) mouse. GL, granular layer. Arrows point to the white matter tracts. Bar = 50 μm.

in spinal cords of the 4-month-old *Nefl*$^{N98S/+}$ as in the 18-month-old *Nefl*$^{N98S/+}$ animals.

When we examined the cerebella of 7-day-old mice, we noticed a clear difference between *Nefl*$^{+/+}$ and *Nefl*$^{N98S/+}$ mice (Fig. 7A and B). There was less labeling in the WM tracts of the *Nefl*$^{N98S/+}$ mice, with punctate labeling in the internal granule layer. Purkinje cell bodies also appear to be stained. In sections from 1-month-old mice, we observed more punctate labeling in

the internal granular layer, although there was still some WM labeling (Fig. 7C). There was no labeling of Purkinje cell bodies. By 4 months of age, there were no clear differences between the labeling patterns of anti-NFL staining of the cerebella of *Nefl*$^{N98S/+}$ and the 18-month-old *Nefl*$^{N98S/+}$ mice (Fig. 7D).

Aggregates of N98S NFL result in the lack of neurofilaments in sciatic nerve and decreased axonal area

Western blots suggested that there was less NFL protein in the sciatic nerves of the *Nefl*$^{N98S/+}$ mice. We therefore performed an electron microscopic analysis of sciatic nerves of 1-year-old animals. As can be seen in the low-power images (Fig. 8A and B), there were fewer neurofilaments in the nerves of the *Nefl*$^{N98S/+}$ mouse compared with *Nefl*$^{+/+}$ mice and the axon diameters appeared to be smaller. At higher power (Fig. 8C and D), it can be seen that the predominant structures in the nerves of the *Nefl*$^{N98S/+}$ mouse (Fig. 8D) were microtubules rather than the abundant neurofilaments that can be observed in the *Nefl*$^{+/+}$ mice (Fig. 8C). These results were in agreement with the immunohistochemistry showing that the neurofilaments were primarily in the cell bodies of the neurons, where they formed aggregates. In contrast, neither the *Nefl*$^{P8R/+}$ nor *Nefl*$^{P8R/P8R}$ mice showed any significant changes in the density of neurofilaments. Unmyelinated axons in the sciatic nerve typically have more microtubules and fewer neurofilaments than myelinated axons (20,21). Electron microscopic analysis of the unmyelinated axons shows that in sections from *Nefl*$^{N98S/+}$ mice, we still see the presence of IFs (Supplementary Material, Fig. S6).

Neurofilament number is usually well correlated with axonal diameter (20,21). We therefore determined the distribution of the axon area for the *Nefl*$^{+/+}$, *Nefl*$^{N98S/+}$ and *Nefl*$^{P8R/+}$ mice. There were no significant differences between the diameters of the axons of the *Nefl*$^{+/+}$ and *Nefl*$^{P8R/+}$ mice, but the axons of the *Nefl*$^{N98S/+}$ mice were considerably smaller (Fig. 9). To determine whether the myelin/axon ratios of the sciatic nerves of the *Nefl*$^{N98S/+}$ mice were changed compared with the *Nefl*$^{+/+}$ mice, we calculated the average *g*-values (fiber area/axon area) for each of the phenotypes (Fig. 9). *Nefl*$^{N98S/+}$ mice had considerably higher *g*-values compared with the both the *Nefl*$^{+/+}$ and *Nefl*$^{P8R/+}$ mice. Using a Kolmogorov–Smirnov (KS test), we confirmed that there was a statistically significant difference between the *Nefl*$^{+/+}$ and the *Nefl*$^{N98S/+}$mice ($P < 0.001$). There was no statistically significant difference between the *Nefl*$^{+/+}$ and the *Nefl*$^{P8R/+}$mice ($P > 0.05$).

Discussion

Mutations in *NEFL* have clearly been linked to CMT2E. The mutations are dominant and span the entire molecule (1). In addition, two recessive mutations resulting in loss of NFL protein cause a severe form of CMT (10,11). Previous studies have produced two

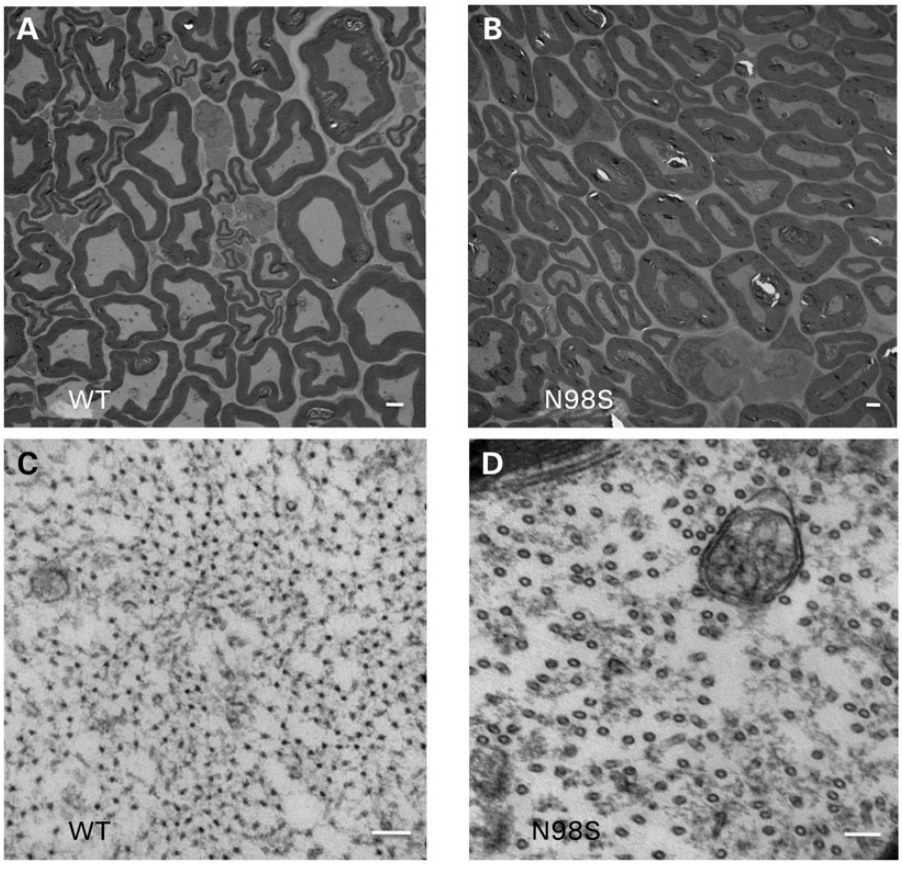

Figure 8. Electron micrographs of sciatic nerves from *Nefl*$^{+/+}$ and *Nefl*$^{N98S/+}$ mice. (**A** and **B**) Low power views of section of sciatic nerves from *Nefl*$^{+/+}$ mouse (A, WT) and *Nefl*$^{N98S/+}$ mouse (B, N98S). (**C** and **D**). High power views of sciatic nerves from *Nefl*$^{+/+}$ mouse (C, WT) and *Nefl*$^{N98S/+}$ mouse (D, N982). At low power (A and B), differences in axon diameter can be observed. At high power (C and D), neurofilaments can be seen in the section from the *Nefl*$^{+/+}$ mouse (C, shown in cross-section) that are missing in the sections from the *Nefl*$^{N98S/+}$ mouse, where they are replaced with microtubules (D). Three sets of animals were analyzed. Bars A and B = 2 μm; C and D = 100 μm.

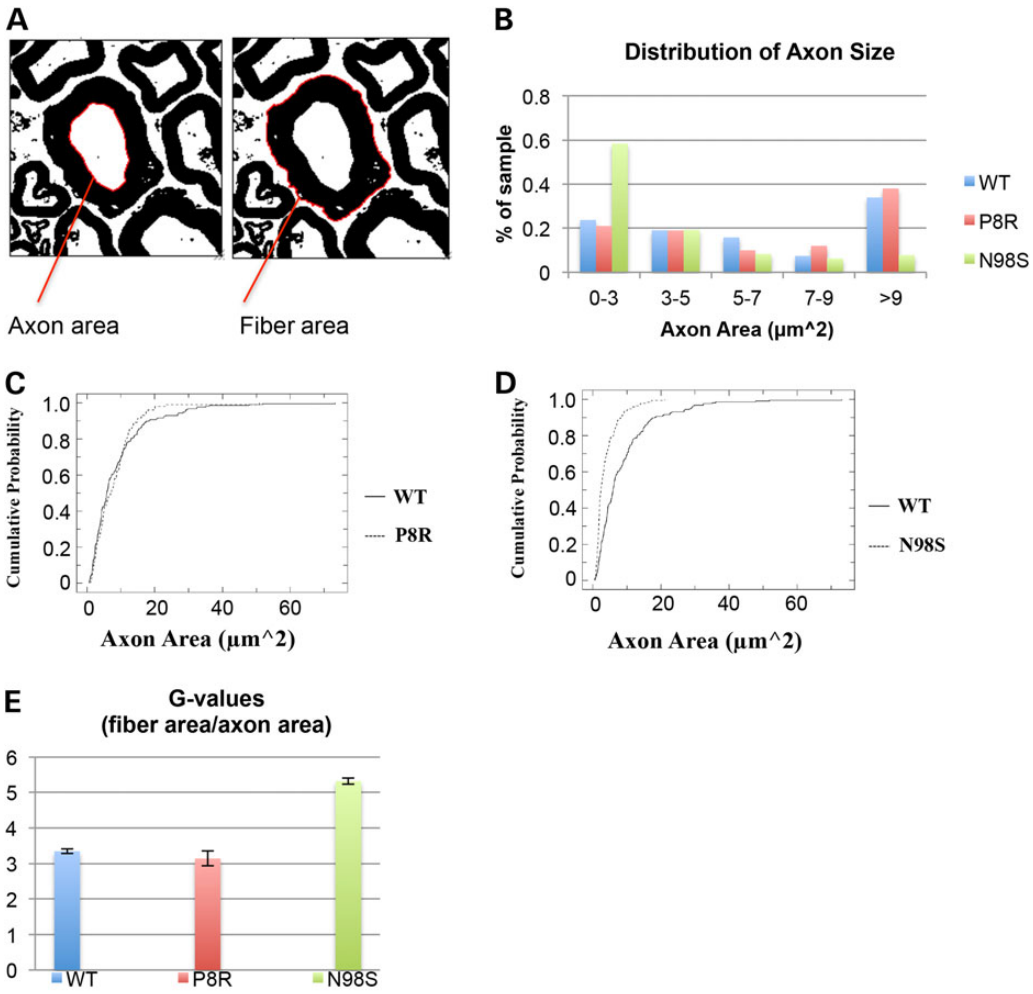

Figure 9. Axon size distribution and *g*-ratios based on the electron micrographs. (**A**) *G* ratio = fiber area/axon area. Axon and fiber areas were measured using the magic wand tool set to scale in ImageJ. (**B**) $Nefl^{+/+}$ and $Nefl^{P8R/+}$ mice show similar distribution of axon sizes, with axons >9 μm^2 occupying the greatest percentage of the sample measured. $Nefl^{N98S/+}$ mice show a different pattern of axon size distribution, with a greater percentage of axons with smaller areas. (**C**) Cumulative distribution of axon areas measured in $Nefl^{+/+}$ and $Nefl^{P8R/+}$ mice. The distributions are not significantly different (Kolmogorov–Smirnov KS test $P > 0.05$). (**D**) Cumulative distribution of axon areas measured in $Nefl^{+/+}$ and $Nefl^{N98S/+}$ mice. The distributions are significantly different (Kolmogorov–Smirnov KS test $P < 0.001$). (**E**) $Nefl^{+/+}$ and $Nefl^{P8R/+}$ mice show similar *g*-ratios axon sizes. $Nefl^{N98S/+}$ mice show a much higher *g*-ratio, indicating that there is more myelin on the axons of the $Nefl^{N98S/+}$ mutant mice; $Nefl^{+/+}$ $n = 215$, $Nefl^{N98S/+}$ $n = 192$, and $Nefl^{P8R/+}$ $n = 100$. Data were pooled from the results from three different mice.

different mutant mouse models with CMT-linked NFL alterations. The Julien laboratory generated mice in which P22S human NFL was expressed under control of a tetracycline-responsive gene system (22). These mice showed aberrant hindlimb posture, hypertrophy of muscle fibers and loss of muscle innervation without neuronal loss. The symptoms were reversible when the mutant gene was turned off, suggesting that therapies aimed at abolishing the abnormal NFL might actually revert the disabilities. However, symptoms were not readily apparent until the mice were 9 months of age. Furthermore, expression of human NFL was <50% of the endogenous WT murine NFL, whereas in the autosomal dominant human disease one would expect that the mutant protein level would be similar to that of WT hNFL. The Garcia laboratory has generated a mouse with an E397K NFL mutant under control of the hNFL promoter (23). In this mouse, symptoms were first observed at 4 months, with aberrant hindlimb deformities, reduced locomotor activity and muscle atrophy. Expression of the human NFL variant was also <50% of endogenous NFL in this transgenic mouse. No inclusions were observed in either of these two mutant mouse models.

We decided that the best way to model the disease was to use a knock-in strategy, replacing one of the copies of the orthologous mouse *Nefl* gene with a mutant allele. We focused on two different mutations. The P8R mutation in the head region of the neurofilament protein is one of the first described mutations and has been identified in a number of families. The age of onset of the disease for patients with the P8R mutations is quite variable but usually in the second or third decade of life. In contrast, the N98S mutation in the rod region of NFL has been described only in sporadic cases with an age of onset of <2 years. Consistent with the early age of onset of the human patients with this mutation, the mutant $Nefl^{N98S/+}$ mice were symptomatic at an early age.

Similar to human patients with the N98S mutation, the symptoms in the $Nefl^{N98S/+}$ mouse were observed quite early. A distinct tremor could be observed as early as 1 month of age. By immunohistochemistry, we were able to observe abnormal

neurofilamentous aggregates labeling in both the cerebellum and the spinal cord as early as post-natal day 7. In addition, more than half of the animals showed hindlimb clasping. In contrast, the *Nefl*$^{P8R/+}$ and the *Nefl*$^{P8R/P8R}$ mice had no observable symptoms, but the *Nefl*$^{P8R/P8R}$ had a clear reduction in the amount of NFL protein, suggesting that this variant protein may be less stable or targeted for degradation. A slow loss of NFL protein in patients with the P8R mutation could account for the late onset symptoms, which would not be observed in an animal with a relatively short lifespan.

There were few if any neurofilaments in the myelinated axons of the sciatic nerves of the *Nefl*$^{N98S/+}$ mice. Instead the nerves were filled with microtubules. The presence of microtubules rather than neurofilaments in neurons of *Nefl*$^{N98S/+}$ mice suggests that these cytoskeletal elements may have compensated for the lack of IFs. Similar results have been observed in the axons of *Nefl*$^{-/-}$ mice (24). The average size of the axons was decreased, but the *g* ratio (ratio of the area of the axon and the axon plus myelin) showed that these although reduced in size, the axons had normal myelin thickness. The unmyelinated axons still show the presence of IFs. Some of these unmyelinated axons are known to contain peripherin as their major IF protein (25), and the mutant N98S NFL may not be present in sufficient amounts in these axons to disrupt the filaments. Knock-out of peripherin in mice also results in a decreased number of unmyelinated fibers, suggesting that it is the primary IF in these fibers (26). The motor neurons of peripherin knock-out mice can be rescued by the overexpression of NFH, showing the interdependence of these neuronal IFs (27) that can all polymerize together to form IFs (28). The striking absence of any neurofilaments in the myelinated axons of the sciatic nerve of the *Nefl*$^{N98S/+}$ mice is similar to the results obtained by two different mouse models, the *Nefl*$^{-/-}$ (24) and the NFH-LacZ mice that lacked neurofilaments in the axons (29). One key difference is that the *Nefl*$^{N98S/+}$ mice have a tremor and show hindlimb clasping, symptoms that were not observed with the other mouse models. These studies suggest that the mutant protein has additional deleterious functions, perhaps as a result of the formation of aggregates in the cell bodies, as well as effects on other organelles and axonal transport. We have previously shown in transfected neuronal cells that CMT-linked mutant NFL proteins cause defects in retrograde and anterograde axonal transport, including mitochondrial transport, as well as fragmentation of the Golgi (30). Defects in mitochondria and axonal abnormalities have also been shown to precede the disruption of the neurofilament network in another study (31). The absence of neurofilaments in the sciatic nerve suggests that the filaments are trapped in the cell body and not transported into the axon. The exact nature of the aggregates is still a matter of debate. Electron microscopic studies that have been performed on neurofilamentous inclusions usually show the presence of tightly packed neurofilaments, rather than broken aggregated filaments (17). The exact consequences of the presence of neurofilamentous aggregates can be variable. In the absence of NFL, overexpression of human NFH resulting in aggregates in transgenic mice caused motor dysfunction, but no motor neuron death. In contrast, overexpression of peripherin resulted in toxic inclusions (32). The difference in phenotype between the neurofilament knock-out mice (24), which have very mild symptoms, and the *Nefl*$^{N98S/+}$ mice reported here also suggest the deleterious effects of the presence of neurofilamentous aggregates.

The tremor that we observe for the *Nefl*$^{N98S/+}$ mice could be due to the effects of the mutant neurofilament in either the spinal cord or the cerebellum. Immunostaining of the cerebella of the *Nefl*$^{N98S/+}$ mice with anti-NFL showed disorganized processes as well as some axonal swellings. Purkinje cell bodies were not affected and double labeling with calbindin antibody showed that Purkinje cell processes were quite normal. Abnormal neurofilament labeling in the cerebellum could be seen as early as P7 for the *Nefl*$^{N98S/+}$ mice.

The only differences that we observed in the the *Nefl*$^{P8R/+}$ or the *Nefl*$^{P8R/P8R\ mice}$ was a lower expression of NFL protein. The lack of any other obvious abnormalities in the *Nefl*$^{P8R/+}$ or the *Nefl*$^{P8R/P8R\ mice}$ is somewhat surprising, especially given that this mutation can result in a rather severe form of CMT1 (8). However, the severity of symptoms in humans varies considerably, so it is likely that genetic background will play a role in the severity of the symptoms seen in mice. Furthermore, additional behavioral assays may reveal abnormalities that we have not observed with our limited assays. One other surprising result is that the phenotype of the *Nefl*$^{N98S/+}$ mice did not progress in severity with further aging. One simple possibility is that the mice live in a rather stress-free environment and that they would do worse in other tests. We have also not quantified neuronal death in these animals as they age. One should further note that NFL knock-out mice have quite a mild phenotype and a normal lifespan. In fact, the *Nefl*$^{N98S/+}$ mice have a much more obvious phenotype. In contrast, humans with no NFL have a much more severe type of CMT than humans with the various mutations (10,11).

In summary, we report on two different knock-in mice with mutations in *Nefl* linked to CMT2E. Neither the *Nefl*$^{P8R/+}$ nor the *Nefl*$^{P8R/P8R}$ mice had a strong phenotype. In contrast, *Nefl*$^{N98S/+}$ mice showed multiple symptoms. In contrast to the P8R mutant mice, *Nefl*$^{N98S/+}$ mice had neurofilamentous inclusions in neuronal cell bodies and axons. There were abnormal neuronal IF networks in the cerebellum and the spinal cord as early as post-natal day 7. These results demonstrate a correlation between the formation of neuronal IFs aggregates and phenotype severity. Furthermore, the phenotype of the *Nefl*$^{N98S/+}$ mice is consistent with the early onset of symptoms in patients with this particular mutation, which is in contrast to the later onset of symptoms in patients with the *NEFL*$^{P8R/+}$ mutation. Finally, these mice will ultimately be very useful in testing of potential therapies for this disease.

Materials and Methods

Generation of *Nefl* P8R and N98S knock-in mice

We used recombination-mediated genetic engineering or recombineering to construct vectors for manipulation of the mouse genome (http://recombineering.ncifcrf.gov/). We obtained a bacterial artificial chromosome (BAC) clone that spans the entire murine *Nefl* gene and modified it using BAC recombineering technology in the following manner: CCG>CGG (P8R) or AAC>AGC (N98S) mutations were introduced into the first exon of the *Nefl* gene and a LNL (Loxp-Neo-Loxp) cassette was inserted in the intron downstream of this exon to generate the 'P8R (or N98S)/neo' *Nefl* allele on the BAC. The introduced mutations were verified by DNA sequencing. Gene-targeting vectors were constructed by retrieving a 5 kb homology arm (5′ to LNL), LNL and a 2 kb short homology arm (end of LNL to 3′) into a plasmid vector carrying the diphtheria toxin alpha chain (DTA) negative selection marker. The LNL cassette conferred G418 resistance during gene targeting in KV1 (129B6 hybrid) embryonic stem (ES) cells, and the DTA cassette provided an autonomous negative selection to reduce the random integration event during gene targeting.

Several targeted ES cells were identified and injected into C57BL/6 blastocysts to generate chimeric mice. Male chimeras were crossed to homozygous *EII*a (cre/cre) females (C57BL/6 background) to transmit the P8R or N98S *Nefl* allele (with the neo cassette removed by Cre recombinase) through the germline. Female mice (F1 generation, likely mosaic) carrying P8R or N98S *Nefl* alleles were then crossed to WT C57BL/6 male to transmit the P8R or N98S *Nefl* allele to the F2 generation.

RT–PCR and western blotting

Animals were sacrificed by CO_2 asphyxiation, and their brains, spinal cords and sciatic nerves were isolated. To examine NFL expression by RT–PCR, total RNA from mouse tissues was isolated with TRIzol reagent (Invitrogen), reverse-transcribed with SuperScript II polymerase (Invitrogen) and the resulting first-strand DNA was amplified with forward primer and reverse primer. To normalize the results, glyceraldehyde 3-phosphate dehydrogenase (GAPDH) was amplified at the same time and ratios were taken between the NFL and GAPDH signals. Total RNA from mouse tissues was isolated with the RNeasy Plus mini kit (Qiagen, Valencia, CA, USA) and treated with RNase-Free DNase Set (Qiagen) according to manufacturer's instructions. RNAs of WT NFL, P8R and N98S were reverse transcribed and a fragment was amplified using OneStep RT-PCR kit (Qiagen).

For western blotting, tissues were homogenized in ice-cold phosphate-buffered saline (PBS) containing 8 M urea and centrifuged in a tabletop microcentrifuge. Concentrations were determined using the Coomassie Protein Assay kit (Thermo Fisher Scientific, Waltham, MA, USA). Ten to twenty-five micrograms of brain and spinal cord protein and 20–25 μg of sciatic nerve protein were separated by SDS-PAGE and transferred to Immobilon-P membrane (Millipore). The membranes were blocked with 5% fat-free milk in PBS/1% Tween-20 and incubated with primary antibodies in blocking solution overnight at 4°C. After washing with PBS/Tween-20, the membrane was incubated with secondary antibodies for 1 h, washed with PBS/Tween-20 and PBS, and the immunoreactive proteins were visualized on the Odyssey infrared scanner (LICOR Biosciences). Intensities of the blot signals were measured in arbitrary units using ImageJ. NFL protein levels were calculated as a ratio between NFL blot signal and the loading control (GAPDH). These ratios were then normalized to WT levels and averaged across gels. Protein samples were collected from two sets of mice and run on gels in triplicate. (Brain: WT: $n = 10$; P8RHet: $n = 9$; P8RHomo: $n = 10$; N98S: $n = 9$; Spinal Cord: WT: $n = 10$; P8RHet: $n = 9$; P8RHomo: $n = 10$; N98S: $n = 9$; Sciatic Nerve: WT: $n = 9$; P8RHet: $n = 8$; P8RHomo: $n = 9$; N98S: $n = 7$). Significance was calculated using a one-tailed, type 3 *t*-test in excel ($^{*}P \leq 0.05$, $^{**}P \leq 0.01$, $^{***}P \leq 0.001$, $^{****}P \leq 0.0001$).

Antibodies

A rabbit polyclonal anti-NFL antibody was previously generated against a 20 amino acid synthetic peptide corresponding to the N-terminus of NFL (anti-NFL-N) (33). The specificity of the labeling was verified using a monoclonal anti-NFL NR4 antibody from Abcam (Cambridge, MA, USA). Anti-GAPDH was purchased from EnCor Biotechnology Inc. (Gainesville, FL, USA) and anti-calbindin D-28k was obtained from SWANT (Switzerland). AlexaFluor-594-goat anti-mouse IgG (H+L) and AlexaFluor-488-goat anti-rabbit IgG (H+L) were used as secondary antibodies for the labeling. 926–68171 IRDye® 680RD Goat anti-Rabbit IgG (H+L) (LICOR) and 827–08364 IRDye 800CW Goat anti-Mouse IgG (H+L) (LICOR) were used as secondary antibodies for western blots.

Labeling

Mice were anesthetized with isofluorane and perfused with 4% paraformaldehyde (PFA) in PBS (pH 7.4). The brain, a section of the spinal cord and the dorsal root ganglia were removed and post fixed in 4% PFA for 2 h before being transferred into PBS. Tissue samples were then embedded in paraffin and cut into 5 μm sections. Sections were incubated at 58°C for 1 h and rehydrated [xylene 10′ × 2, 100% ethanol 10′ × 2, 95% ethanol 5′, 75% ethanol 5′, 50% ethanol 5′, distilled H20 3′, [PBS with 0.1% Tween-20 (PBST) 5′ × 2]. For antigen retrieval, slides were placed in preheated Trylogy for 30′. Sections were rinsed again with PBST and were blocked for 30′ with 10% goat serum in PBS/Tween-20. Overnight incubation was performed at 4°C with primary antibodies (NFL-N polyclonal, 1 : 1000; Calbindin monoclonal, 1 : 500). The following day, sections were brought back to room temperature, rinsed with PBS/Tween-20 (8′ × 2) and incubated for 30′ with two antibodies (Goat-Anti-Rabbit & Goat-anti-mouse, H+L chain, 1 : 1000). Slides were mounted using Aquamount and digital images were taken with a Zeiss Axioplan 2 microscope equipped with camera AxioCam with Axiovision software (Zeiss).

Shaking and clasping assays

Mice were held upside down by the tail for a 30 s interval. An observer noted any shaking or clasping during this interval. To prevent bias, the tester was not aware of the genotype of the mice.

Electron microscopy

Animals were anesthetized and perfused with 4% paraformaldehyde and 2% glutaraldehyde in 0.1 M cacodylate buffer, pH 7.4. Tissue blocks were immersed in the same fixative for 24 h at 4°C, rinsed in cacodylate buffer and post-fixed in 1% osmium tetroxide for 2 h. After three washes with cacodylate buffer, each sample was dehydrated in a graded series of ethanol and embedded in Epon-Araldite resin. Plastic sections (1 μm) were stained with toluidine blue and examined for light microscopy. Ultrathin sections were stained with uranyl acetate and lead.

Axon and fiber area measurements

Axon and Fiber areas were measured from several electron micrographs using the magic wand tool set to scale in ImageJ, *g*-value = outer fiber area/internal axon area.

Supplementary Material

Supplementary Material is available at *HMG* online.

Acknowledgements

We thank Dr Neilla Gracias, Dr Markel Olabarria Larizgoitia and Mr Joe Chan for their assistance with some of the experiments and Dr James Goldman for advise on the neuroanatomy.

Conflict of Interest statement. None declared.

Funding

This work was supported by an ARRA grant from the National Institutes of Health (RC1NS068131) to R.K.H.L. and H.J.W. and a grant from the Muscular Dystrophy Association (MDA2550838) to R.K.H.L.

References

1. Liem, R.K. and Messing, A. (2009) Dysfunctions of neuronal and glial intermediate filaments in disease. *J. Clin. Invest.*, **119**, 1814–1824.
2. Shy, M.E. and Patzko, A. (2011) Axonal Charcot-Marie-Tooth disease. *Curr. Opin. Neurol.*, **24**, 475–483.
3. Suter, U. and Scherer, S.S. (2003) Disease mechanisms in inherited neuropathies. *Nat. Rev. Neurosci.*, **4**, 714–726.
4. Dyck, P.J. and Lambert, E.H. (1968) Lower motor and primary sensory neuron diseases with peroneal muscular atrophy. II. Neurologic, genetic, and electrophysiologic findings in various neuronal degenerations. *Arch. Neurol.*, **18**, 619–625.
5. Dyck, P.J. and Lambert, E.H. (1968) Lower motor and primary sensory neuron diseases with peroneal muscular atrophy. I. Neurologic, genetic, and electrophysiologic findings in hereditary polyneuropathies. *Arch. Neurol.*, **18**, 603–618.
6. Reilly, M.M., Murphy, S.M. and Laura, M. (2011) Charcot-Marie-Tooth disease. *J. Peripher. Nerv. Syst.*, **16**, 1–14.
7. Liem, R.K. (1993) Molecular biology of neuronal intermediate filaments. *Curr. Opin. Cell. Biol.*, **5**, 12–16.
8. Jordanova, A., De Jonghe, P., Boerkoel, C.F., Takashima, H., De Vriendt, E., Ceuterick, C., Martin, J.J., Butler, I.J., Mancias, P., Papasozomenos, S. *et al.* (2003) Mutations in the neurofilament light chain gene (NEFL) cause early onset severe Charcot-Marie-Tooth disease. *Brain*, **126**, 590–597.
9. Mersiyanova, I.V., Perepelov, A.V., Polyakov, A.V., Sitnikov, V. F., Dadali, E.L., Oparin, R.B., Petrin, A.N. and Evgrafov, O.V. (2000) A new variant of Charcot-Marie-Tooth disease type 2 is probably the result of a mutation in the neurofilament-light gene. *Am. J. Hum. Genet.*, **67**, 37–46.
10. Abe, A., Numakura, C., Saito, K., Koide, H., Oka, N., Honma, A., Kishikawa, Y. and Hayasaka, K. (2009) Neurofilament light chain polypeptide gene mutations in Charcot-Marie-Tooth disease: nonsense mutation probably causes a recessive phenotype. *J. Hum. Genet.*, **54**, 94–97.
11. Yum, S.W., Zhang, J., Mo, K., Li, J. and Scherer, S.S. (2009) A novel recessive Nefl mutation causes a severe, early-onset axonal neuropathy. *Ann. Neurol.*, **66**, 759–770.
12. Ching, G. and Liem, R. (1998) Roles of head and tail domains in (alpha)-internexin's self-assembly and coassembly with the neurofilament triplet proteins. *J. Cell Sci.*, **111**, 321–333.
13. Perez-Olle, R., Jones, S.T. and Liem, R.K. (2004) Phenotypic analysis of neurofilament light gene mutations linked to Charcot-Marie-Tooth disease in cell culture models. *Hum. Mol. Genet.*, **13**, 2207–2220.
14. Perez-Olle, R., Leung, C.L. and Liem, R.K. (2002) Effects of Charcot-Marie-Tooth-linked mutations of the neurofilament light subunit on intermediate filament formation. *J. Cell Sci.*, **115**, 4937–4946.
15. Fabrizi, G.M., Cavallaro, T., Angiari, C., Bertolasi, L., Cabrini, I., Ferrarini, M. and Rizzuto, N. (2004) Giant axon and neurofilament accumulation in Charcot-Marie-Tooth disease type 2E. *Neurology*, **62**, 1429–1431.
16. Yoshihara, T., Yamamoto, M., Hattori, N., Misu, K., Mori, K., Koike, H. and Sobue, G. (2002) Identification of novel sequence variants in the neurofilament-light gene in a Japanese population: analysis of Charcot-Marie-Tooth disease patients and normal individuals. *J. Peripher. Nerv. Syst.*, **7**, 221–224.
17. Ching, G.Y., Chien, C.L., Flores, R. and Liem, R.K. (1999) Overexpression of alpha-internexin causes abnormal neurofilamentous accumulations and motor coordination deficits in transgenic mice. *J. Neurosci.*, **19**, 2974–2986.
18. Benito-Leon, J. and Louis, E.D. (2006) Essential tremor: emerging views of a common disorder. *Nat. Clin. Pract. Neurol.*, **2**, 666–678.
19. Enderlin, S., Norman, A.W. and Celio, M.R. (1987) Ontogeny of the calcium binding protein calbindin D-28k in the rat nervous system. *Anat. Embryol. (Berl.)*, **177**, 15–28.
20. Friede, R.L. and Samorajski, T. (1970) Axon caliber related to neurofilaments and microtubules in sciatic nerve fibers of rats and mice. *Anat. Rec.*, **167**, 379–387.
21. Hoffman, P.N., Griffin, J.W. and Price, D.L. (1984) Control of axonal caliber by neurofilament transport. *J. Cell Biol.*, **99**, 705–714.
22. Dequen, F., Bomont, P., Gowing, G., Cleveland, D.W. and Julien, J.P. (2008) Modest loss of peripheral axons, muscle atrophy and formation of brain inclusions in mice with targeted deletion of gigaxonin exon 1. *J. Neurochem.*, **107**, 253–264, 21.
23. Shen, H., Barry, D.M., Dale, J.M., Garcia, V.B., Calcutt, N.A. and Garcia, M.L. (2011) Muscle pathology without severe nerve pathology in a new mouse model of Charcot-Marie-Tooth disease type 2E. *Hum. Mol. Genet.*, **20**, 2535–2548.
24. Zhu, Q., Coouillard-Despres, S. and Julien, J.-P. (1997) Delayed maturation of regenerating myelinated axons in mice lacking neurofilaments. *Exper. Neurol.*, **148**, 299–316.
25. Parysek, L.M., McReynolds, M.A., Goldman, R.D. and Ley, C.A. (1991) Some neural intermediate filaments contain both peripherin and the neurofilament proteins. *J. Neurosci. Res.*, **30**, 80–91.
26. Lariviere, R.C., Nguyen, M.D., Ribeiro-da-Silva, A. and Julien, J.P. (2002) Reduced number of unmyelinated sensory axons in peripherin null mice. *J. Neurochem.*, **81**, 525–532.
27. Beaulieu, J.M. and Julien, J.P. (2003) Peripherin-mediated death of motor neurons rescued by overexpression of neurofilament NF-H proteins. *J. Neurochem.*, **85**, 248–256.
28. Yuan, A., Sasaki, T., Kumar, A., Peterhoff, C.M., Rao, M.V., Liem, R.K., Julien, J.P. and Nixon, R.A. (2012) Peripherin is a subunit of peripheral nerve neurofilaments: implications for differential vulnerability of CNS and peripheral nervous system axons. *J. Neurosci.*, **32**, 8501–8508.
29. Eyer, J. and Peterson, A. (1994) Neurofilament-deficient axons and perikaryal aggregates in viable transgenic mice expressing a neurofilament-beta-galactosidase fusion protein. *Neuron*, **12**, 389–405.
30. Perez-Olle, R., Lopez-Toledano, M.A., Goryunov, D., Cabrera-Poch, N., Stefanis, L., Brown, K. and Liem, R.K. (2005) Mutations in the neurofilament light gene linked to Charcot-Marie-Tooth disease cause defects in transport. *J. Neurochem.*, **93**, 861–874.
31. Tradewell, M.L., Durham, H.D., Mushynski, W.E. and Gentil, B.J. (2009) Mitochondrial and axonal abnormalities precede disruption of the neurofilament network in a model of charcot-marie-tooth disease type 2E and are prevented by heat shock proteins in a mutant-specific fashion. *J. Neuropath. Exp. Neurol*, **68**, 642–652.
32. Beaulieu, J.M., Jacomy, H. and Julien, J.P. (2000) Formation of intermediate filament protein aggregates with disparate effects in two transgenic mouse models lacking the neurofilament light subunit. *J. Neurosci.*, **20**, 5321–5328.
33. Kaplan, M.P., Chin, S.S., Macioce, P., Srinawasan, J., Hashim, G. and Liem, R.K. (1991) Characterization of a panel of neurofilament antibodies recognizing N-terminal epitopes. *J. Neurosci. Res.*, **30**, 545–554.